molecular pharmaceutics

articles

Evaluation of the Microstructure of Semicrystalline Solid Dispersions

Qing Zhu,[†] Lynne S. Taylor,[‡] and Michael T. Harris*,[†]

School of Chemical Engineering and Department of Industrial and Physical Pharmacy, Purdue University, West Lafayette, Indiana 47907

Received March 31, 2010; Revised Manuscript Received June 10, 2010; Accepted June 15, 2010

Abstract: As a result of an increase in the number of emerging therapies with dissolution limited bioavailability, formulation strategies such as solid dispersions that enhance the rate of solubilization are of interest. In this study, the microstructure of solid dispersions prepared with polyethylene glycol (PEG) and four model compounds with different physicochemical properties was evaluated using a variety of experimental techniques. Solid dispersions were prepared by fusion and evaluated using small-angle X-ray scattering (SAXS), powder X-ray diffraction (PXRD), atomic force microscopy (AFM), optical microscopy and differential scanning calorimetry (DSC). SAXS results indicated that aceclofenac and chlorpropamide solid dispersions favored the interlamellar incorporation of the drug in the PEG matrix. Optical microscopy did not show any evidence of interspherulitic accumulation for any of the model compounds. Haloperidol was highly crystalline in the dispersions, whereas evidence of amorphous material was found for the other model compounds. Results indicated that both the crystallization tendency of the drug and its solubility in amorphous regions of PEG played important roles in determining the location (i.e., interlamellar, interfibrillar or interspherulitic regions) and size of the drug domains within the dispersion.

Keywords: Polyethylene glycol; structure; solid dispersion; solubility; interlamellar; powder X-ray diffraction; small-angle X-ray scattering

Introduction

Several methods have been employed to enhance the bioavailability of active pharmaceutical ingredients (APIs) with low aqueous solubility including micronization,[1] dispersion of the API in a carrier (typically a polymer),[2] and chemical modification through the formation of prodrugs.[3,4] Among these methods, solid dispersions[2] have received extensive attention as a potential approach to increase the dissolution rate of the API.[5−8] However, there are still limitations that restrict the widespread application of this technique. A major concern is the reproducibility and consistency of the physicochemical properties of the solid

* Corresponding author. Mailing address: Purdue University, School of Chemical Engineering, 480 Stadium Mall Drive, West Lafayette, IN 47907. E-mail: mtharris@purdue.edu. Tel: +1-765-494-4050. Fax: +1-765-494-0805.

† School of Chemical Engineering.

‡ Department of Industrial and Physical Pharmacy.

(1) Atkinson, R. M.; Bedford, C.; Child, K. J.; Tomich, E. G. Effect of particle size on blood Griseofulvin-levels in man. *Nature* **1962**, *193*, 588–589.

(2) Sekiguchi, K.; Obi, N. Studies on absorption of eutectic mixture. I. A comparison of the behavior of eutectic mixture of sulfathiazole and that of ordinary sulfathiazole in man. *Chem. Pharm. Bull.* **1961**, *9*, 866–872.

(3) Albert, A. Chemical aspects of selective toxicity. *Nature* **1958**, *182*, 421–423.

(4) Sinkula, A. A.; Yalkowsky, S. H. Rationale for design of biologically reversible drug derivatives: prodrugs. *J. Pharm. Sci.* **1975**, *64* (2), 181–210.

(5) Chiou, W. L.; Riegelman, S. Pharmaceutical applications of solid dispersion systems. *J. Pharm. Sci.* **1971**, *60*, 1281–1302.

(6) Serajuddin, A. T. M. Solid dispersion of poorly water-soluble drugs: early promises, subsequent problems, and recent breakthroughs. *J. Pharm. Sci.* **1999**, *88*, 1058–1066.

(7) Leuner, C.; Dressman, J. Improving drug solubility for oral delivery using solid dispersions. *Eur. J. Pharm. Biopharm.* **2000**, *50*, 47–60.

(8) Craig, D. Q. M. The mechanisms of drug release from solid dispersions in water-soluble polymers. *Int. J. Pharm.* **2002**, *231*, 131–144.

10.1021/mp1000907
Published on Web 06/15/2010

dispersions during manufacturing, scale-up and storage.[5,6] Additionally, the mechanism by which the dissolution rate is enhanced is still unclear.[8] The physicochemical properties and the dissolution mechanisms are likely to be closely related to both the solid dispersion microstructure and the phase behavior. Solid dispersions are frequently prepared using highly water-soluble polymers as the carrier.[8] The carrier polymers can be amorphous or partially crystalline. Amorphous polymers are typically used to inhibit crystallization of the API, producing an amorphous dispersion.[6,7] In contrast, when semicrystalline polymers are used, the API can be crystalline, amorphous or partially crystalline and, if present in a metastable state, the phase behavior may vary as a function of time and preparation conditions.[5,6,8−11]

Polyethylene glycol (PEG) is a highly water-soluble, low melting point, semicrystalline polymer that has attracted considerable interest as a carrier matrix for solid dispersions.[5,7] The structure of pure PEG has been widely investigated and well characterized.[12−16] In addition, the solidification behavior of PEG in the presence of high molecular weight additives (i.e., other polymers) has been extensively probed using techniques such as small-angle X-ray scattering (SAXS) and differential scanning calorimetry (DSC).[17−21] However, there are fewer studies investigating how the microstructure is altered in blends of PEG prepared with low molecular weight additives. The solid-state structure of PEG 4000/monoolein mixtures was investigated by Mahlin et al. using SAXS.[22] It was found that monoolein was partly intercalated in the amorphous regions of PEG, and a second phase of monoolein was detected at above 10% monoolein. Unga et al. found that incorporation of parabens in the interlamellar domains of PEG appeared to be related to the solubility of different parabens in PEG.[23] It also has been found that the properties of lipid additives can affect the crystallization of PEG.[24] Qian et al. observed that nanosized API crystals were formed in spray-dried API/PEG systems.[25] Further characterization of the microstructure of different API/PEG systems and elucidation of the fundamental physicochemical processes that govern microstructural evolution are still needed in order to better understand this type of solid dispersion.

The purpose of this study was to probe the microstructure of different API/PEG dispersions after solidification. Model APIs with different crystallization tendencies and interactions with PEG were selected and comelted with PEG. The crystallization behavior and the microstructure of the API/PEG solid dispersions were investigated with powder X-ray diffraction (PXRD), SAXS and atomic force microscopy (AFM).

Experimental Section

Materials and Sample Preparation. Model APIs, chlorpropamide (CPM) and haloperidol (HLP), were obtained from Sigma-Aldrich Inc. (St. Louis, MO), while aceclofenac (ACF), and loratadine (LRT) were purchased from Attix Pharmachem Canada (Toronto, Ontario). PEG with a molecular weight 3350 was a kind gift from Dow Chemical (Midland, MI). Mixtures of the API and PEG were comelted and allowed to solidify at predetermined temperatures. Following solidification, the samples were stored in desiccators at low relative humidity for 24 h prior to analysis.

(9) Craig, D. Q. M. Polyethylene glycols and drug release. *Drug Dev. Ind. Pharm.* **1990**, *16*, 2501–2526.
(10) Lloyd, G. R.; Craig, D. Q. M.; Smith, A. An investigation into the melting behavior of binary mixes and solid dispersions of paracetamol and PEG 4000. *J. Pharm. Sci.* **1997**, *86* (9), 991–996.
(11) Lloyd, G. R.; Craig, D. Q. M.; Smith, A. An investigation into the production of paracetamol solid dispersions in PEG 4000 using hot stage differential interference contrast microscopy. *Int. J. Pharm.* **1997**, *158*, 39–46.
(12) Baltá Calleja, F. J.; Hay, I. L.; Keller, A. Diffraction effects in single crystals and spherulites of poly(ethylene oxide). *Colloid Polym. Sci.* **1966**, *209*, 128–135.
(13) Arlie, P. J. P.; Spegt, P. A.; Skoulios, A. E.; Etude. de la cristallisation des polymères I Structure lamellaire de polyoxyéthylènes de faible masse moléculaire. *Macromol. Chem. Phys.* **1966**, *99*, 160–174.
(14) Arlie, P. J. P.; Spegt, P.; Skoulios, A. Etude de la cristallisation des polymères II. Structure lamellaire et repliement des chaînes du polyoxyéthylène. *Macromol. Chem. Phys.* **1967**, *104*, 212–229.
(15) Buckley, C. P.; Kovacs, A. J. Melting behavior of low molecular weight poly(ethylene-oxide) fractions 2. Folded chain crystals. *Colloid Polym. Sci.* **1976**, *254* (8), 695–715.
(16) Cheng, S. Z. D.; Zhang, A. Q.; Chen, J. H.; Heberer, D. P. Nonintegral and integral folding crystal growth in low-molecular mass poly(ethylene oxide) fractions. I. Isothermal lamellar thickening and thinning. *J. Polym. Sci., Part B: Polym. Phys.* **1991**, *29*, 287–297.
(17) Silvestre, C.; Karasz, F. E.; Macknight, W. J.; Martuscelli, E. Morphology of poly(ethylene oxide)/poly(vinyl acetate) blends. *Eur. Polym. J.* **1987**, *23* (10), 745–751.
(18) Silvestre, C.; Cimmino, S.; Martuscelli, E. Poly(ethylene oxide)/poly(methyl methacrylate) blends: influence of tacticity of poly(methyl methacrylate) on blend structure and miscibility. *Polymer* **1987**, *28*, 1190–1199.
(19) Russell, T. P.; Ito, H. Neutron and X-ray scattering studies on semicrystalline polymer blends. *Macromolecules* **1988**, *21*, 1703–1709.
(20) Talibuddin, S.; Wu, L.; Runt, J. Microstructure of melt-miscible, semicrystalline polymer blends. *Macromolecules* **1996**, *29*, 7527–7535.
(21) Utracki, L. A. *Polymer Blends Handbook*, 1st ed.; Kluwer Academic Publishers: Dordrecht, The Netherlands, 2002; pp 203−212.
(22) Mahlin, D.; Ridell, A.; Frenning, G.; Engström, S. Solid-state characterization of PEG4000/monoolein mixtures. *Macromolecules* **2004**, *37*, 2665–2667.
(23) Unga, J.; Tajarobi, F.; Norder, O.; Frenning, G.; Larsson, A. Relating solubility data of parabens in liquid PEG 400 to the behavior of PEG 4000-parabens solid dispersions. *Eur. J. Pharm. Biopharm.* **2009**, *73*, 260–268.
(24) Unga, J.; Matsson, P; Mahlin, D. Understanding polymer-lipid solid dispersions-The properties of incorporated lipids govern the crystallization behavior of PEG. *Int. J. Pharm.* **2010**, *386*, 61–70.
(25) Qian, F.; Tao, J.; Desikan, S.; Hussain, M.; Smith, R. L. Mechanistic investigation of Pluronic® based nano-crystalline drug-polymer solid dispersions. *Pharm. Res.* **2007**, *24*, 1551–1560.

Differential Scanning Calorimetry (DSC). Samples were analyzed using a TA Instruments Q2000 differential scanning calorimeter (TA Instruments, New Castle, DE) with a nitrogen purge of 50 mL/min. The instrument was calibrated for temperature and enthalpy/cell constant by using indium (TA Instruments, New Castle, DE). The samples were analyzed in the aluminum pans with sealed lids and were first equilibrated at −80 °C and then heated up above the melting point of the pure API at rates of both 2 and 20 °C/min.

The fraction of crystalline PEG in the sample, x_c, was approximated from the following equation:[22]

$$x_c = \frac{\Delta H_m^{PEG,sample}}{\Delta H_m^{PEG,crystal} X_{PEG}} \quad (1)$$

where $\Delta H_m^{PEG,sample}$ is the heat of fusion for PEG in the sample, $\Delta H_m^{PEG,crystal}$ is the heat of fusion for a perfect PEG crystal whereby a value of 205 J/g was used,[26] and X_{PEG} is the weight percent of PEG in the samples.

Small-Angle X-ray Scattering (SAXS). SAXS experiments were run on a Molecular Metrology SAXS instrument equipped with 2-D Gabriel design, gas filled, proportional type detector (125 mm diameter active area). The X-ray source is a BEDE Microsource X-ray generator with a Cu Kα radiation (λ = 1.54 Å), 3 pinhole collimation. The samples with thickness of approximately 1 mm were fixed onto the standard sample holder by Scotch tape, and the scattering was collected at room temperature under vacuum for 6−10 h. The intensity was calculated by dividing the total count by the collection time and by the ratio of the flux of the scattered beam to the flux of the incident beam.

Powder X-ray Diffraction (PXRD). The samples were cryogenically milled (SPEX SamplePrep model 6750) at 10 Hz for two cycles, each cycle consisting of 0.2 min of milling followed by 0.2 min of cool-down. The resultant powder was mounted on a sample holder. The PXRD patterns were collected using a Scintag diffractometer with a Si Peltier detector and a Cu Kα radiation (λ = 1.54 Å) source. The voltage was 40 kV, and the current was 44 mA. The samples were scanned for $2\theta = 4-44°$, at speed of 1° per min.

Atomic Force Microscopy (AFM). AFM experiments were carried out at room temperature using a NanoScope IV multimode AFM (Digital Instruments, Santa Barbara, CA), employing a J-scanner with a phosphorus doped Si probe (frequency, 248−325 kHz; spring constant, 20−80 N/m). The tapping mode was employed in air at the cantilever's resonant frequency using a probe to obtain the phase images.

Hot-Stage Microscopy. The pure components were placed on glass slides on the Nikon Eclipse E600 polarized light microscope (Nikon Inc., Melville, NY) equipped with Linkam THMS 600 hot-stage (Linkam Scientific Instruments Ltd., Surrey, U.K.). The samples were heated at 10 °C/min to above the melting point of the pure component, and then cooled to room temperature under ambient conditions. Following cooling, photomicrographs were obtained after 24 h.

Results and Discussion

Estimation of the Solubility of the API in PEG at 25 °C. It has been suggested that there is a correlation between the solubility of a small molecule additive in PEG and its subsequent effect on the microstructure of solidified PEG.[23] Therefore it was of interest to estimate the solubility of the model compounds at 25 °C. Since this is below the melting point of PEG, the solubility estimate is for the supercooled liquid of PEG. The solubility of various model APIs in molten PEG has been reported previously.[27] The solubility of each API at 25 °C was estimated using the Van't Hoff equation[28]

$$\frac{d \ln x}{dT} = \frac{\Delta H_f}{RT^2} \quad (2)$$

where x is the mole fraction of API in PEG solution, ΔH_f is the heat of fusion, and T is the temperature. HLP and LRT were predicted to have negligible solubility (less than 1%), while the estimated solubility of ACF was around 23% w/w after converting to mass fraction, and that of CPM in PEG was around 26% w/w.

Phase of the API in API/PEG Dispersions. The phase behavior of each pure API and PEG following melting and cooling to room temperature was determined using polarized microscopy. HLP and PEG crystallized immediately after cooling. CPM crystallized within a few hours, while ACF and LRT were amorphous after cooling and had not crystallized after a 24 h storage period. However, when ACF was melted in an aluminum pan and analyzed using DSC after 24 h storage at room temperature, a very small melting peak was observed, indicating that ACF had partially crystallized (although this could have occurred during the course of the DSC experiment).

The phase of the API in the dispersion following solidification was determined by PXRD of samples after storage for 24 h. In the HLP/PEG solid dispersions, HLP existed as a crystalline phase which had the same diffraction pattern as the starting material (Figure 1a). CPM can form several polymorphs.[29−31] The commercially obtained form of CPM was polymorph A. When the CPM/PEG system solidified,

(26) Vidotto, P. G.; Lévy, D.; Kovacs, A. J. Cristallisation et fusion des polymères autoensemencés I. Polybutène-1, polyéthylène et polyoxyéthylène de haute masse moléculaire. *Colloid Polym. Sci.* **1969**, *230*, 289–305.

(27) Baird, J. A.; Taylor, L. S. Evaluation and modeling of the eutectic composition of various drug-polyethylene glycol solid dispersions. *Pharm. Dev. Technol.* **2010**, DOI: 10.3109/10837450903584936.

(28) Connors, K. A. 2002. *Thermodynamics of Pharmaceutical Systems - An Introduction for Students of Pharmacy*; Wiley-Interscience: Hoboken, NJ, 2002; pp 118−119.

(29) Vemavarapu, C.; Mollan, M. J.; Needham, T. E. Crystal doping aided by rapid expansion of supercritical solutions. *AAPS PharmSciTech* **2002**, *3* (4), article 29.

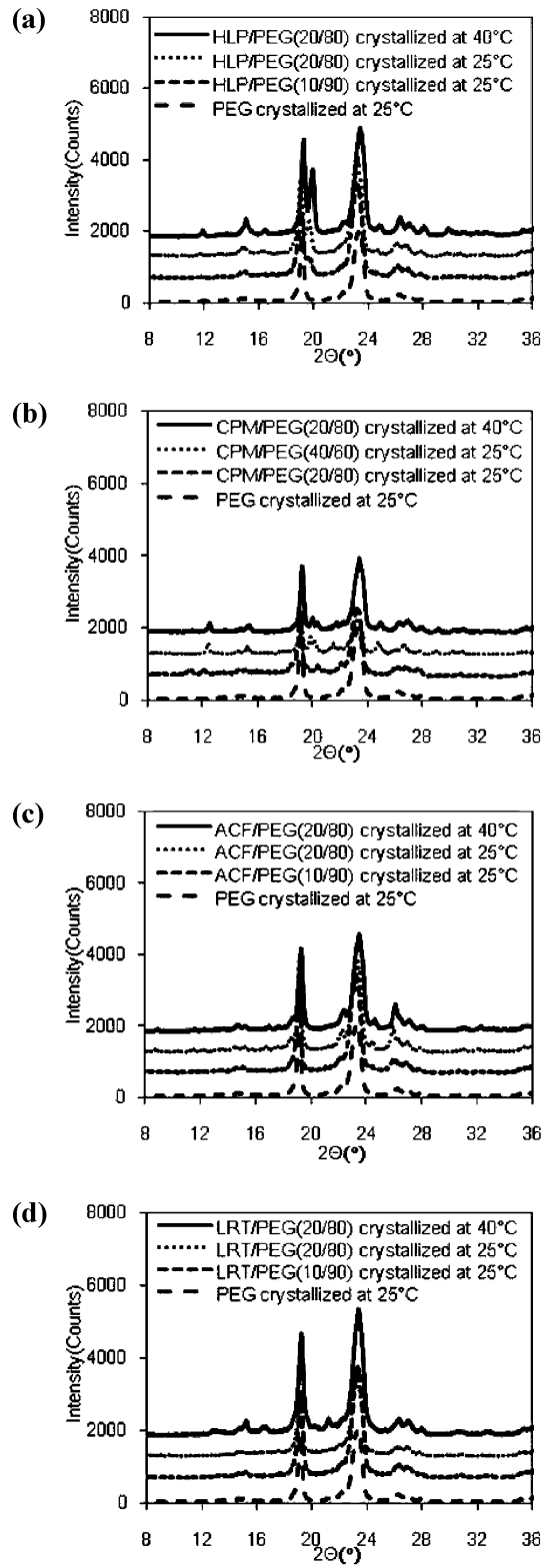

Figure 1. PXRD patterns: (a) HLP/PEG dispersions; (b) CPM/PEG dispersions; (c) ACF/PEG dispersions; (d) LRT/PEG dispersions.

CPM polymorph B was identified from the PXRD pattern in the dispersion with 20% w/w CPM prepared at 25 °C (Figure 1b). Both polymorph B and polymorph C were found in the CPM/PEG (40/60) dispersion prepared at 25 °C and the CPM/PEG (20/80) dispersion prepared at 40 °C. For ACF/PEG (20/80) solid dispersions prepared at 25 and 40 °C (Figure 1c), the diffraction pattern from ACF was the same as that of the commercially obtained ACF, albeit with a weaker intensity than from a physical mixture at the same composition. No diffraction peak arising from LRT was apparent in LRT/PEG solid dispersions crystallized at 25 °C, suggesting that LRT existed as a disordered form in this dispersion (Figure 1d). In contrast, when the dispersion was crystallized at 40 °C, appreciable LRT crystallinity could be observed after 24 h. In all cases, the lattice structure of PEG in the dispersions was the same as for PEG crystallized in the absence of the API.

Microstructure of PEG. The structure of the PEG matrix needs to be considered to understand the location and size range of the API in API/PEG solid dispersions. PEG is a highly crystallizable polymer and has a typical spherulitic structure. Based on the enthalpy of fusion value measured for PEG 3350 by DSC, the weight percent of crystalline PEG for PEG3350 after crystallization at room temperature was estimated as 90%. At the beginning of the crystallization process, it has been reported that PEG exists as nonintegral folding (NIF) lamellae.[16] With time, a more stable structure evolves, with the PEG chains becoming either extended or folded with an integer number, n times.[14−16,32−34] The theoretical chain length of PEG with a MW of 3350 is approximately 21.2 nm,[33] which means the long period of the extended chain integral folding (IF) lamellar structure should be around 21.2 nm, while that of the once-folded chain IF lamella should be around 10.6 nm.[15,16,33] The structure of PEG in the presence and absence of API can be evaluated using SAXS as described previously.[17−21]

The Lorentz-corrected SAXS results (Figure 2) of pure PEG (MW 3350), crystallized at different temperatures, showed multiple diffraction peaks at different scattering vectors. From Bragg's law $L = 2\pi/q$ (where L is the long period, and q is the scattering vector), the diffraction peak

(30) Chesalov, Y. A.; Baltakhinov, V. P.; Drebushchak, T. N.; Boldyreva, E. V.; Chukanov, N. V.; Drebushchak, V. A. FT-IR and FT-Raman spectra of five polymorphs of chlorpropamide. Experimental study and ab initio calculations. *J. Mol. Struct.* **2008**, *891*, 75–86.

(31) Drebushchak, V. A.; Drebushchak, T. N.; Chukanov, N. V.; Boldyreva, E. V. Transitions among five polymorphs of chlorpropamide near the melting point. *J. Therm. Anal. Cal.* **2008**, *93* (2), 343–351.

(32) Kovacs, A. J.; Gonthier, A. Crystallization and fusion of self-seeded polymers II. Growth rate, morphology and isothermal thickening of single crystals of low molecular weight poly(ethylene-oxide) fractions. *Colloid Polym. Sci.* **1972**, *250*, 530–551.

(33) Cheng, S. Z. D.; Chen, J. H.; Zhang, A. Q.; Barley, J. S. Isothermal thickening and thinning processes in low molecular weight poly(ethylene oxide) fractions crystallized from the melt: 2. Crystals involving more than one fold. *Polymer* **1992**, *33* (6), 1140–1149.

(34) Cheng, S. Z. D.; Bu, H. S.; Wunderlich, B. Molecular segregation and nucleation of poly(ethylene oxide) crystallized from the melt. III. Morphological study. *J. Polym. Sci., Part B: Polym. Phys.* **1988**, *26*, 1947–1964.

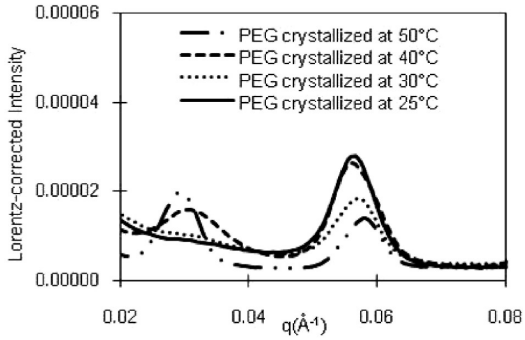

Figure 2. SAXS data for PEG crystallized at different temperatures.

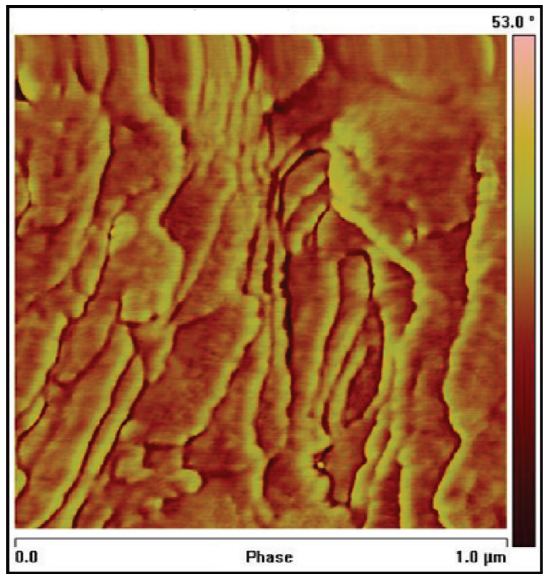

Figure 3. AFM phase image of PEG crystallized at 25 °C.

at around $q = 0.029$ Å^{-1} corresponded to a long period L of 21.7 nm. A second, more intense peak at $q = 0.057$ Å^{-1} was also present. If this diffraction peak is only due to the second order diffraction of the first peak ($q = 0.029$ Å^{-1}), the intensity ratio of these two peaks should be the same when varying the crystallization temperature. However, the intensity ratio changed at different crystallization temperatures, which indicated that this diffraction peak arose partly due to the presence of another lamellar structure, whereby the long period L of this lamella was 11.0 nm. These two lamellae can thus be assigned to the extended-chain IF lamella ($L = 21.7$ nm) and the once-folded IF lamella ($L =$ 11.0 nm). The intensity ratios of two diffraction peaks indicated that the extended chain lamella dominated when the PEG was crystallized at higher temperatures, while the once-folded chain lamella dominated for the lower crystallization temperatures. These results are in agreement with literature reports.[14−16] PEG structure following crystallization was also investigated by AFM. The phase image (Figure 3) clearly showed the lamellae packing.

Microstructure of the API/PEG Dispersions. The microstructure of PEG following solidification with the four model compounds was evaluated using SAXS and AFM. As

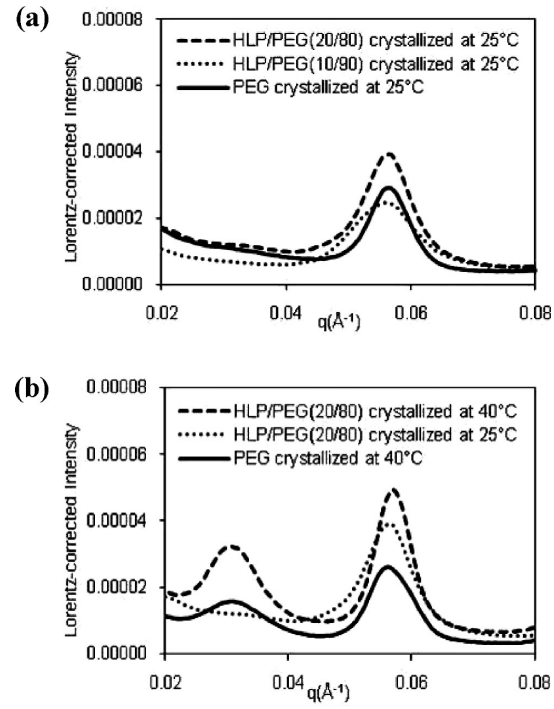

Figure 4. SAXS data: (a) different compositions of HLP/PEG dispersions; (b) HLP/PEG dispersions crystallized at different temperatures.

described above, the various model compounds have different estimated solubilities in supercooled liquid PEG and also different crystallization tendencies, both as pure compounds and following comelting with PEG. It is anticipated that this variation in API phase behavior will affect the crystallization behavior and microstructure of PEG.

The SAXS profile of HLP/PEG dispersions crystallized at 25 °C (Figure 4a) had a diffraction peak at $q = 0.057$ Å^{-1}; this peak occurred at the same position and had a similar width to the peak occurring in pure PEG. In addition, diffraction peaks for HLP/PEG dispersions crystallized at 40 °C (Figure 4b) occurred at the same scattering vectors as for pure PEG crystallized at 40 °C. These results indicated that the long period of PEG in a dispersion with HLP was similar to that found in the pure polymer, i.e. that the API had minimal impact on the polymer microstructure. The long period is the sum of the thickness of the crystalline lamellae and amorphous layers.[21] If the API exists in the amorphous layer, termed interlamellar incorporation, it would result in the increase of the amorphous layer and the long period. Since no change was seen in the length of the long period, it appears likely that HLP was excluded from the PEG interlamellar regions (PEG amorphous phases are between lamellae). DSC results indicated that there was no significant change of the position and shape of the melting peak for PEG in the PEG/HLP dispersions compared to pure PEG, supporting this supposition. AFM image (Figure 5) indicated that HLP formed discrete particles in the submicrometer range. Optical microscopy showed that the spherulites were space-filling with no evidence of HLP interspherulitic

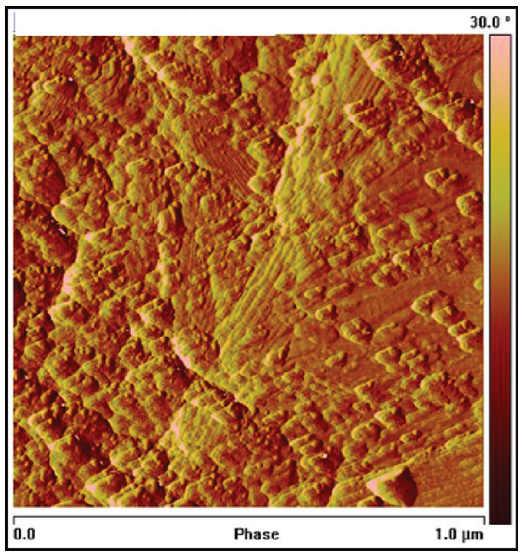

Figure 5. AFM phase image of HLP/PEG (10/90) dispersion crystallized at 25 °C.

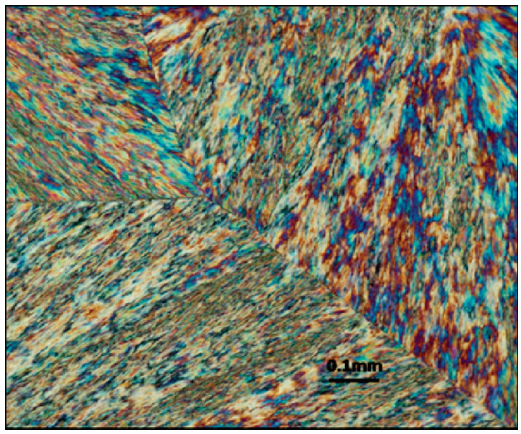

Figure 6. Photomicrograph obtained under polarized light showing a HLP/PEG (20/80) dispersion crystallized at 25 °C.

accumulation (Figure 6). Therefore, based on the evidence presented above, the most likely location of HLP was in the interfibrillar regions.

In contrast to the HLP/PEG system, when 20% CPM was comelted with PEG to form CPM/PEG dispersions, the diffraction peak in the small-angle X-ray scattering profile (Figure 7a) shifted to a smaller scattering vector ($q \approx 0.053$ Å^{-1}), which corresponded to a larger long period ($L = 11.8$ nm). The diffraction peak shifted even further to the smaller scattering vector ($q \approx 0.045$ Å^{-1}) for a 40% CPM loading prepared at 25 °C, and the long period increased to approximately 14.0 nm. A similar trend of shifting to a smaller scattering vector was also observed for CPM/PEG (20/80) dispersion prepared at 40 °C (Figure 7b). It should be noted that mixing of CPM with PEG decreased the melting temperature of the CPM/PEG system by a few degrees (<3 °C). This means that the extent of supercooling has changed for this system, which can potentially affect the lamellar thickness.[14,20] However, since a decrease in supercooling by as little as 3 °C has been observed to have

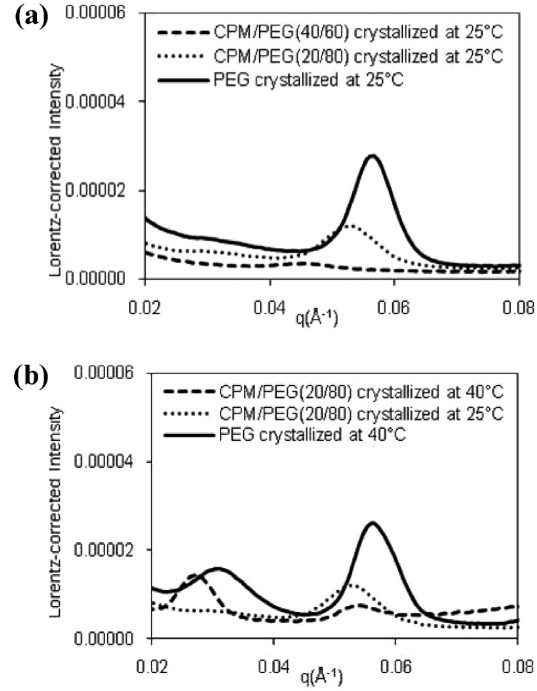

Figure 7. SAXS data: (a) different compositions of CPM/PEG dispersions; (b) CPM/PEG dispersions crystallized at different temperatures.

a negligible effect on the long period of PEG,[14,34] the increase of the long period when adding CPM in PEG cannot be accounted for by a change in the extent of supercooling. The results thus indicated that a portion of chlorpropamide might exist within the interlamellar region of the PEG carrier.

DSC provided further confirmation of the molecular level mixing of PEG and CPM when a dispersion containing 40% CPM was evaluated. For this solid dispersion, a glass transition (T_g) event was detected at −25 °C (no T_g could be seen for the 20% CPM dispersion, presumably due to the small signal). The glass transition temperature of pure CPM was found to be 16.8 °C. The depression of the T_g event to −25 °C upon forming CPM/PEG dispersions indicated that a portion of CPM mixed at the molecular level with PEG. The amount of the API that is mixed with the amorphous PEG can be approximated from the Fox equation[35]

$$\frac{1}{T_g} = \frac{w_1}{T_{g1}} + \frac{1 - w_1}{T_{g2}} \qquad (3)$$

where T_g is the glass transition of the mixture, w_1 is the weight percent of component one, and T_{g1} and T_{g2} are the glass transitions of components one and two respectively. Assuming a T_g of −64 °C for pure PEG,[36] the calculated composition for the molecular mixture in the amorphous PEG

(35) Fox, T. G. Influence of diluent and of copolymer composition on the glass transition temperature of a polymer system. *Bull. Am. Phys. Soc.* **1956**, *1*, 123.

(36) Brandrup, J.; Immergut, E. H.; Grulke, E. A.; Abe, A.; Bloch, D. R. *Polymer Handbook*, 4th ed.; Wiley-Interscience: New York, 1999; pp VI/226.

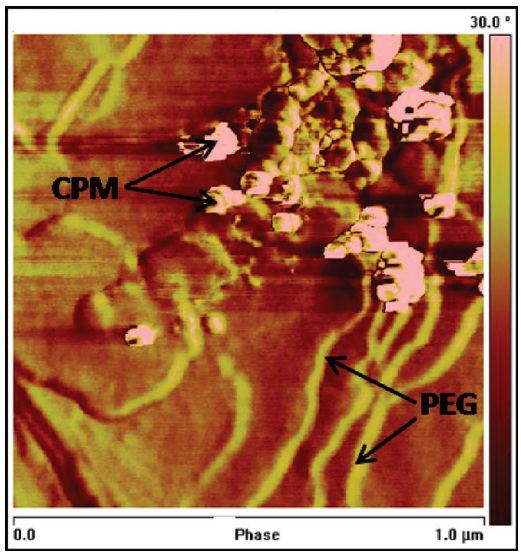

Figure 8. AFM phase image of CPM/PEG (20/80) dispersion crystallized at 25 °C.

region (interlamellar region) was 56%/44% (CPM/PEG w/w). Approximately 19% of the total CPM was mixed with the amorphous PEG in the interlamellar region of PEG.

A further piece of evidence supporting the supposition that CPM is mixed with PEG is the decrease in the intensity of the PEG diffraction peak in the SAXS data. The electron density for the PEG crystalline lamella is 0.676 mol/cm^3, the electron density is 0.611 mol/cm^3 for the PEG amorphous fraction.[20] The density of amorphous chlorpropamide is 1.31 g/cm^3, and the molar mass is 276.74 g/mol. There is 0.00473 mol of CPM in 1 cm^3 of amorphous CPM. Since there are 144 electrons in 1 CPM molecule, 1 cm^3 of amorphous CPM contains 0.682 mol of electrons. Therefore, the electron density was calculated to be 0.682 mol/cm^3 for amorphous CPM. The electron density of an amorphous phase composed of 56% CPM and 44% PEG was predicted to increase to 0.651 mol/cm^3 when loading 40% CPM in PEG. The decreased electron density contrast between the crystalline phase and the amorphous layer explained the observed reduction in intensity of the PEG diffraction peak in the scattering profile when CPM was dispersed with PEG.[37,38] In addition to the presence of CPM in the interlamellar regions, AFM image (Figure 8) showed that a portion of the CPM existed as relatively larger domains. Optical image (Figure 9) did not show any evidence of interspherulitic accumulation.

The amount of API in the interlamellar region can also be estimated from the change in the long period upon addition of CPM. As estimated from the melting enthalpy, pure PEG was around 90% w/w or 89% v/v crystalline

(37) Chen, H. L.; Liu, H. H.; Lin, J. S. Microstructure of semicrystalline poly(L-lactide)/poly(4-vinylphenol) blends evaluated from SAXS absolute intensity measurement. *Macromolecules* **2000**, *33*, 4856–4860.

(38) Shieh, Y. T.; Lin, Y. G.; Chen, H. L. Effect of supercritical CO_2 on phase structure of PEO/PVAc blends evaluated from SAXS absolute intensity measurement. *Polymer* **2002**, *43*, 3691–3698.

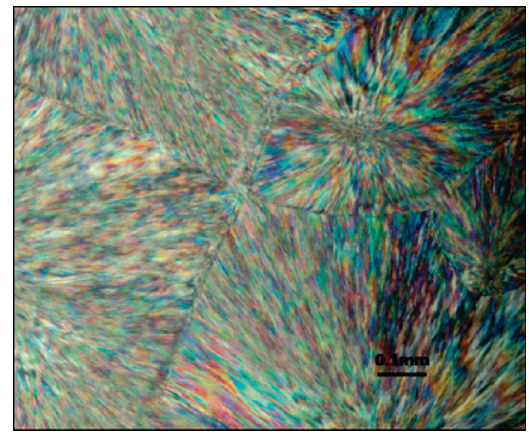

Figure 9. Photomicrograph obtained under polarized light showing a CPM/PEG (40/60) solid dispersion crystallized at 25 °C.

(100% crystalline PEG: $\rho = 1.24$ g/cm^3, 100% amorphous PEG: $\rho = 1.12$ g/cm^3), and the estimated crystallinity was essentially unaltered when cocrystallized with CPM based on the DSC results. The length of the amorphous phase is $11.0 \times (1-89\%) = 1.2$ nm, assuming that the linear crystallinity is the same as bulk crystallinity. When blending with 20% CPM, the long period was increased by 0.8 nm, and this increase was caused by the incorporation of CPM into the amorphous phase of PEG. The volume ratio among crystalline PEG lamellae, amorphous PEG and CPM in the amorphous region between crystalline lamellae is thus 9.8:1.2:0.8, assuming that the volume is additive. Using the densities (amorphous CPM: $\rho = 1.31$ g/cm^3) and converting to mass ratios, approximately 30% of the total CPM present in the blend was estimated to be present in the interlamellar region. This estimate is in reasonable agreement with the value estimated from the DSC data. At 40% CPM loading, a similar calculation can be carried out in principle, but the peak intensity was lower and the precise position of the peak was difficult to determine.

The SAXS profile of the 10/90 ACF/PEG solid dispersion (Figure 10a) demonstrated that the long period of PEG increased to 13 nm in the presence of the API, suggesting that ACF also underwent interlamellar incorporation in the PEG carrier following comelting and solidification, since the melting point was decreased by only 1 °C at this composition.[27] No distinct diffraction peak could be observed for the ACF/PEG (20/80) dispersion prepared at 25 °C while a diffraction peak shift from $q = 0.029$ Å^{-1} (pure PEG crystallized at 40 °C) to $q = 0.027$ Å^{-1} was noted when the dispersion was prepared at 40 °C with 20% ACF (Figure 10b). From DSC experiments conducted on ACF/PEG dispersion containing 20% ACF prepared at 25 °C (this was the minimum level of API for which a T_g was observed), it was estimated that the composition for the ACF/PEG mixture in the amorphous PEG region was 61%/39%. Thus around 63% of the 20% ACF presented was mixed with PEG in the interlamellar region based on the glass transition temperature of pure ACF ($T_g = 16.3$ °C) and ACF dispersed in PEG (T_g

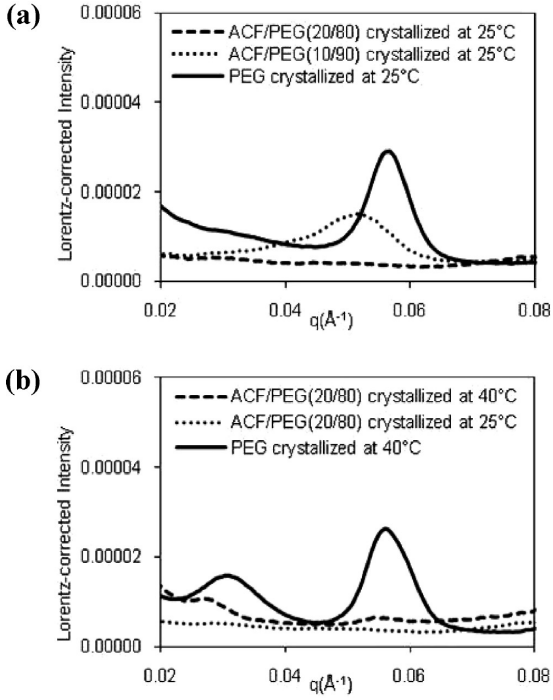

Figure 10. SAXS data: (a) different compositions of ACF/PEG dispersions; (b) ACF/PEG dispersions crystallized at different temperatures.

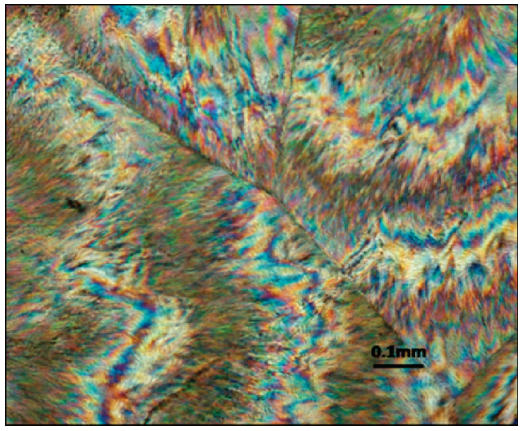

Figure 11. Photomicrograph obtained under polarized light showing a ACF/PEG (20/80) solid dispersion crystallized at 25 °C.

= −21.2 °C). The other portion of ACF was presumed to exist in the interfibrillar region of PEG since optical images showed that the spherulites were space filling (Figure 11). As for CPM, the diffraction peak in the scattering profile was reduced in intensity in the presence of ACF, presumably as a result of the reduced electron density contrast between the crystalline and disordered phases. The electron density for amorphous ACF is 0.716 mol/cm^3 (ρ = 1.39 g/cm^3), which results in an estimated electron density of 0.675 mol/cm^3 for an amorphous phase composed of 61%ACF and 39% PEG (ACF/PEG (20/80) dispersion). Thus the electron density difference between the disordered phase containing a mixture of amorphous ACF and amorphous PEG and that

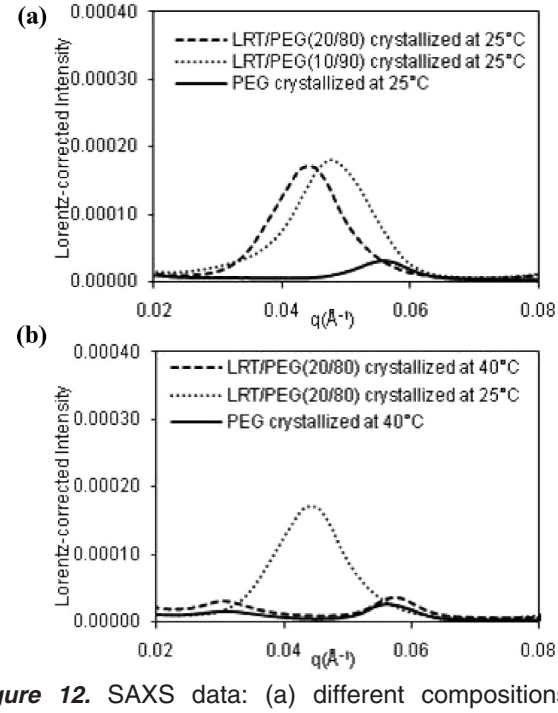

Figure 12. SAXS data: (a) different compositions of LRT/PEG dispersions; (b) LRT/PEG dispersions crystallized at different temperatures.

of the crystalline PEG was less than the contrast between pure amorphous PEG and crystalline PEG.

For LRT/PEG dispersions solidified at 25 °C, the long period increased dramatically to 13.5 cm upon adding 10% LRT to the PEG matrix, and increased to 14.6 cm at a 20% LRT loading (Figure 12a). Because the glass transition of LRT is 34 °C, which is much higher than for the other systems, it was of interest to compare this behavior to that for dispersions solidified above the T_g. Interestingly, there was no change of the long period for LRT/PEG dispersions prepared at 40 °C compared to that for pure PEG crystallized at the same temperature (Figure 12b). This is most likely because LRT crystallized, presumably due to the increased molecular mobility imparted by the higher temperature and the low solubility of this compound in PEG. In contrast, when the LRT vitrified into a glassy solid following solidification at room temperature, it appeared to have affected the crystallization behavior of PEG. DSC results showed that the melting temperatures for pure PEG were around 53 °C (once-folded lamella) and 59 °C (extended lamella).[16] The LRT/PEG dispersions with 20% LRT prepared at 25 °C showed a very broad melting peak below 50 °C and another peak at 59 °C, whereby the melting peak below 50 °C is most likely due to modified crystalline material which resulted from the addition of LRT to PEG. LRT/PEG dispersions prepared at 40 °C did not show the presence of a melting peak below 50 °C and had a similar DSC profile (Figures 13a and 13b) to pure PEG. Further evidence for the exclusion of LRT from the interlamellar region is provided by the increase of the intensities of the scattering peaks in the presence and absence of LRT. Different from

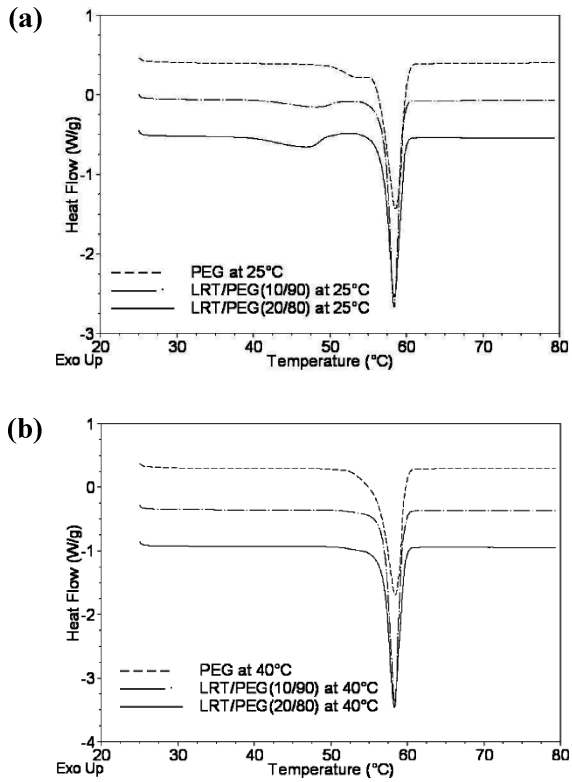

Figure 13. DSC thermograms of LRT/PEG dispersions solidified at (a) 25 °C and (b) 40 °C.

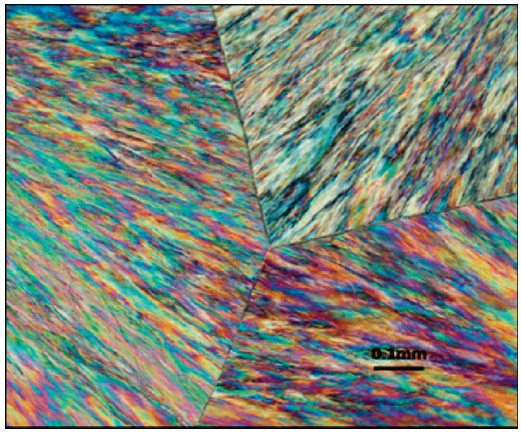

Figure 14. Photomicrograph obtained under polarized light showing a LRT/PEG (20/80) solid dispersion crystallized at 25 °C.

the CPM/PEG or ACF/PEG dispersions, the intensities of diffraction peaks in the scattering profiles of LRT/PEG were not reduced on increasing the concentration of loratadine in the dispersion. Since the electron density of amorphous LRT is 0.648 mol/cm^3, the electron density contrast between the amorphous layer and crystalline lamella should be decreased if LRT is in the interlamellar region of PEG spherulites composed of once folded integral folding lamellae. AFM images did not show interpretable trends for the LRT/PEG dispersions, and no LRT was observed in the interspherulitic region of PEG (Figure 14). The evidence suggested that a more complicated structure was formed for LRT/PEG dispersions when solidified at temperatures lower than the glass transition of LRT, Further study on this system is needed.

It is known from the polymer literature that, for a miscible amorphous component/rapidly crystallizing polymer (e.g., PEG) system, the degree of exclusion of the amorphous component from the PEG crystalline regions, whether it is interlamellar, interfibrillar or interspherulitic region, depends on the crystallization rate of PEG, the mobility of the second component (determined by the blend T_g), and the presence or absence of any specific interaction between the two components.[20,21,24,39−41] The majority of systems described in the literature describe polymer blends. The difference between amorphous polymer/PEG blends and the API/PEG systems is that the diameter of gyration of the amorphous polymer relative to the separation between the crystalline lamellae is usually large enough that its confinement in the interlamellar regions is entropically unfavorable; this is not the case for the small molecules.[20] Since the model APIs are small molecules, there should be a lower entropic driving force to exit from the interlamellar region of PEG. Therefore, it might be expected that, if crystallization of the API does not occur, interlamellar association might occur. From the results presented above, it is clear that the location of the API in the PEG and the microstructure of the API/PEG dispersions varied considerably, depending on the properties of the APIs. The easiest system to understand is the HLP/PEG dispersion which consists of crystallizing polymer and a rapidly crystallizing small molecule. This system cocrystallized to a crystalline API phase and a semicrystalline polymer which had a similar structure to the pure polymer. Thus, in this instance, the additive did not affect the lamellar structure of the polymer due to its rapid phase separation as a crystalline solid. The other model compounds investigated in this study show a lower tendency to crystallize and appear to have a much larger effect on polymer microstructure. It also appears that the solubility of the API in amorphous PEG and specific intermolecular interaction might be of importance. It has been reported in some studies that intermolecular interactions should favor interlamellar incorporation.[20] However, Talibuddin et al. and Kuo et al. have pointed out that stronger intermolecular interactions between the amorphous component and the crystalline polymer decreased the growth rate of the crystalline polymer, which resulted in more time for the amorphous component to diffuse away from the interlamellar region of the crystalline polymer.[20,41] Both CPM and ACF are known to form hydrogen bonds with PEG,[27] and it was qualitatively observed using polarized light

(39) Keith, H. D.; Padden, F. J. Spherulitic crystallization from the melt. I. Fractionation and impurity segregation and their influence on crystalline morphology. *J. Appl. Phys.* **1964**, *35*, 1270–1285.
(40) Stein, R. S.; Khambatta, F. B.; Warner, F. P.; Russell, T.; Escala, A.; Balizer, E. X-ray and optical studies of the morphology of polymer blends. *J. Polym. Sci., Polym. Symp.* **1978**, *63*, 313–328.
(41) Kuo, S. W.; Chan, S. C.; Chang, F. C. Effect of hydrogen bonding strength on the microstructure and crystallization behavior of crystalline polymer blends. *Macromolecules* **2003**, *36*, 6653–6661.

microscopy that the addition of either CPM or ACF did decrease the growth rate of PEG. Furthermore, both of these compounds have low T_gs. Therefore, mobility is expected to be high at the crystallization temperature, which might be expected to favor diffusion away from the interlamellar regions. However, the results show that interlamellar incorporation appears to be favored for these compounds. This outcome probably also results from the slow crystallization tendency of these compounds, and their solubility in PEG−ACF with a higher solubility in PEG and a lower tendency to crystallize showed the greater extent of interlamellar incorporation. In contrast, the behavior of LRT dispersions was very much dependent on the crystallization temperature. It is also important to note that, for the ACF and CPM dispersions, the APIs appear to exist in at least two regions of the polymer, interlamellar and interfibrillar, and that the domain sizes of these different regions are likely to vary considerably, from the nanometric scale in the interlamellar region to the submicrometer or micrometer size in the interfibrillar region. Furthermore, given the partially crystalline nature of the API in the dispersions, and the metastable form of the polymer crystals, the structure of these systems is likely to change with time if either the API or the polymer undergoes additional crystallization. While the results of this study serve to highlight the inherent complexity of API/PEG dispersions, they also provide a starting point to understand the reasons for the often noted changes in structure and performance of PEG based dispersions as a function of preparation technique and storage time.

Conclusions

PEG (MW 3350) formed different types of lamellae following crystallization, depending on the crystallization temperature. Once-folded lamella dominated at room temperatures. When solid dispersions were formed with PEG and different APIs, the location and phase of the API in PEG varied. For slowly crystallizing APIs with high solubility in PEG, incorporation in the interlamellar region of PEG spherulites, as well as in interfibrillar regions, was inferred. In contrast, haloperidol, a rapidly crystallizing compound, was excluded from the interlamellar region. Loratadine, with a low solubility in PEG, showed more complex phase behavior that depended on the crystallization temperature. This study highlights the complex nature of API/PEG dispersions and the interplay between API−polymer specific interactions, crystallization tendency and preparation temperature.

Acknowledgment. We thank Prof. Stephen Z. D. Cheng (The University of Akron), Prof. James Runt (The Pennsylvania State University) and Dr. Denny Mahlin (Uppsala University) for helpful discussion and suggestion. We acknowledge the National Science Foundation Engineering Research Center for Structured Organic Particulate Systems (NSF ERC-SOPS) (EEC-0540855) for financial support.

MP1000907